HAL open science

Observation of a Magnetic Switchback in the Solar Corona

Daniele Telloni, Gary P. Zank, Marco Stangalini, Cooper Downs, Haoming Liang, Masaru Nakanotani, Vincenzo Andretta, Ester Antonucci, Luca Sorriso-Valvo, Laxman Adhikari, et al.

To cite this version:

Daniele Telloni, Gary P. Zank, Marco Stangalini, Cooper Downs, Haoming Liang, et al.. Observation of a Magnetic Switchback in the Solar Corona. The Astrophysical journal letters, 2022, 936, 10.3847/2041-8213/ac8104 . insu-03846981

HAL Id: insu-03846981

https://insu.hal.science/insu-03846981v1

Submitted on 10 Nov 2022

HAL is a multi-disciplinary open access archive for the deposit and dissemination of scientific research documents, whether they are published or not. The documents may come from teaching and research institutions in France or abroad, or from public or private research centers.

L'archive ouverte pluridisciplinaire **HAL**, est destinée au dépôt et à la diffusion de documents scientifiques de niveau recherche, publiés ou non, émanant des établissements d'enseignement et de recherche français ou étrangers, des laboratoires publics ou privés.

Distributed under a Creative Commons Attribution 4.0 International License

The Astrophysical Journal Letters, 936:L25 (9pp), 2022 September 10 https://doi.org/10.3847/2041-8213/ac8104
© 2022. The Author(s). Published by the American Astronomical Society.
OPEN ACCESS

Observation of a Magnetic Switchback in the Solar Corona

Daniele Telloni[1,34], Gary P. Zank[2,3,34], Marco Stangalini[4], Cooper Downs[5], Haoming Liang[2], Masaru Nakanotani[2], Vincenzo Andretta[6], Ester Antonucci[1], Luca Sorriso-Valvo[7,8], Laxman Adhikari[2], Lingling Zhao[2], Raffaele Marino[9], Roberto Susino[1], Catia Grimani[10,11], Michele Fabi[10,11], Raffaella D'Amicis[12], Denise Perrone[4], Roberto Bruno[12], Francesco Carbone[13], Salvatore Mancuso[1], Marco Romoli[14], Vania Da Deppo[15], Silvano Fineschi[1], Petr Heinzel[16], John D. Moses[17], Giampiero Naletto[18], Gianalfredo Nicolini[1], Daniele Spadaro[19], Luca Teriaca[20], Federica Frassati[1], Giovanna Jerse[21], Federico Landini[1], Maurizio Pancrazzi[1], Giuliana Russano[6], Clementina Sasso[6], Ruggero Biondo[1,22], Aleksandr Burtovoi[23], Giuseppe E. Capuano[19,24], Chiara Casini[15,25], Marta Casti[27], Paolo Chioetto[15,25], Yara De Leo[20,24], Marina Giarrusso[14,19], Alessandro Liberatore[1,26], David Berghmans[28], Frédéric Auchère[29], Regina Aznar Cuadrado[20], Lakshmi P. Chitta[20], Louise Harra[30,31], Emil Kraaikamp[28], David M. Long[32], Sudip Mandal[20], Susanna Parenti[29], Gabriel Pelouze[29], Hardi Peter[20], Luciano Rodriguez[28], Udo Schühle[20], Conrad Schwanitz[30,31], Phil J. Smith[32], Cis Verbeeck[28], and Andrei N. Zhukov[28,33]

[1] National Institute for Astrophysics, Astrophysical Observatory of Torino, Via Osservatorio 20, I-10025 Pino Torinese, Italy; daniele.telloni@inaf.it
[2] Center for Space Plasma and Aeronomic Research, University of Alabama in Huntsville, Huntsville, AL 35805, USA
[3] Department of Space Science, University of Alabama in Huntsville, Huntsville, AL 35805, USA
[4] Italian Space Agency, Via del Politecnico snc, I-00133 Roma, Italy
[5] Predictive Science Inc., San Diego, CA 92121, USA
[6] National Institute for Astrophysics, Astronomical Observatory of Capodimonte, Salita Moiariello 16, I-80131 Napoli, Italy
[7] Swedish Institute of Space Physics, Ångström Laboratory, Lägerhyddsvägen 1, SE-751 21 Uppsala, Sweden
[8] National Research Council, Institute for the Science and Technology of Plasmas, Via Amendola 122/D, I-70126 Bari, Italy
[9] Laboratoire de Mécanique des Fluides et d'Acoustique, Centre National de la Recherche Scientifique, École Centrale de Lyon, Université Claude Bernard Lyon 1, INSA de Lyon, F-69134 Écully, France
[10] University of Urbino Carlo Bo, Department of Pure and Applied Sciences, Via Santa Chiara 27, I-61029 Urbino, Italy
[11] National Institute for Nuclear Physics, Section in Florence, Via Bruno Rossi 1, I-50019 Sesto Fiorentino, Italy
[12] National Institute for Astrophysics, Institute for Space Astrophysics and Planetology, Via del Fosso del Cavaliere 100, I-00133 Roma, Italy
[13] National Research Council, Institute of Atmospheric Pollution Research, c/o University of Calabria, I-87036 Rende, Italy
[14] University of Florence, Department of Physics and Astronomy, Via Giovanni Sansone 1, I-50019 Sesto Fiorentino, Italy
[15] National Research Council, Institute for Photonics and Nanotechnologies, Via Trasea 7, I-35131 Padova, Italy
[16] Czech Academy of Sciences, Astronomical Institute, Fričova 298, CZ-25165 Ondřejov, Czech Republic
[17] National Aeronautics and Space Administration, Headquarters, Washington, DC 20546, USA
[18] University of Padua, Department of Physics and Astronomy, Via Francesco Marzolo 8, I-35131 Padova, Italy
[19] National Institute for Astrophysics, Astrophysical Observatory of Catania, Via Santa Sofia 78, I-95123 Catania, Italy
[20] Max Planck Institute for Solar System Research, Justus-von-Liebig-Weg 3, D-37077 Göttingen, Germany
[21] National Institute for Astrophysics, Astronomical Observatory of Trieste, Località Basovizza 302, I-34149 Trieste, Italy
[22] University of Palermo, Department of Physics and Chemistry—Emilio Segrè, Piazza del Parlamento 1, I-90134 Palermo, Italy
[23] National Institute for Astrophysics, Astrophysical Observatory of Arcetri, Largo Enrico Fermi 5, I-50125 Firenze, Italy
[24] University of Catania, Department of Physics and Astronomy, Via Santa Sofia 64, I-95123 Catania, Italy
[25] Centre of Studies and Activities for Space "Giuseppe Colombo", Via Venezia 15, I-35131 Padova, Italy
[26] Jet Propulsion Laboratory, California Institute of Technology, Pasadena, CA 91109, USA
[27] The Catholic University of America at the National Aeronautics and Space Administration, Goddard Space Flight Center, Greenbelt, MD 20771, USA
[28] Solar-Terrestrial Centre of Excellence, Solar Influences Data Analysis Center, Royal Observatory of Belgium, Avenue Circulaire 3, B-1180 Brussels, Belgium
[29] Université Paris-Saclay, Centre National de la Recherche Scientifique, Institut d'Astrophysique Spatiale, Bâtiment 121, F-91405 Orsay, France
[30] Physical Meteorological Observatory in Davos, World Radiation Center, Dorfstrasse 33, CH-7260 Davos Dorf, Switzerland
[31] Swiss Federal Institute of Technology in Zürich, Hönggerberg Campus, Wolfgang-Pauli-Strasse 27, CH-8093 Zürich, Switzerland
[32] Mullard Space Science Laboratory, University College London, Holmbury St. Mary, RH5 6NT Dorking, UK
[33] Skobeltsyn Institute of Nuclear Physics, Moscow State University, 119992 Moscow, Russia
Received 2022 June 5; revised 2022 July 6; accepted 2022 July 7; published 2022 September 12

Abstract

Switchbacks are sudden, large radial deflections of the solar wind magnetic field, widely revealed in interplanetary space by the Parker Solar Probe. The switchbacks' formation mechanism and sources are still unresolved, although candidate mechanisms include Alfvénic turbulence, shear-driven Kelvin–Helmholtz instabilities, interchange reconnection, and geometrical effects related to the Parker spiral. This Letter presents observations from the Metis coronagraph on board a Solar Orbiter of a single large propagating S-shaped vortex, interpreted as the first evidence of a switchback in the solar corona. It originated above an active region with the related loop system bounded by open-field regions to the east and west. Observations, modeling, and theory provide strong arguments in favor of the interchange reconnection origin of switchbacks. Metis measurements suggest that the initiation of the switchback may also be an indicator of the origin of slow solar wind.

[34] These authors contributed equally to this work.

Original content from this work may be used under the terms of the Creative Commons Attribution 4.0 licence. Any further distribution of this work must maintain attribution to the author(s) and the title of the work, journal citation and DOI.

Unified Astronomy Thesaurus concepts: Solar corona (1483); Solar magnetic reconnection (1504); Solar magnetic fields (1503); Magnetohydrodynamics (1964); Solar coronal waves (1995); Slow solar wind (1873)

1. Introduction

The solar wind is a continuous flow of charged particles streaming from the Sun's outermost atmosphere, the solar corona, into interplanetary space (Hundhausen 1972). It is characterized by the coexistence of large-scale structures of solar origin, turbulent fluctuations, magnetohydrodynamic (MHD) and kinetic plasma waves, and instabilities, and associated with physical processes such as magnetic reconnection, shocks, and a broad range of kinetic processes, which result in particle heating and energization (Bruno & Carbone 2013).

The solar wind acceleration mechanisms, its complex dynamics and interaction with the solar magnetic field, and the observed plasma heating are still outstanding questions in heliophysics. One interesting solar wind feature emerging from in situ spacecraft measurements is the puzzling existence of abrupt, temporary magnetic field reversals, named magnetic switchbacks.

First observed in the outer heliosphere by the Ulysses spacecraft in high-latitude fast solar wind (Balogh et al. 1999; Yamauchi et al. 2004), switchbacks are markedly Alfvénic, pressure-balanced structures, characterized by constant temperature and magnetic field magnitude, and associated with substantial acceleration of the plasma. Later analysis of Helios data in the ecliptic fast solar wind showed an abundance of such structures in the inner heliosphere (Horbury et al. 2018). More recently, extensive measurements by the Parker Solar Probe (PSP, Fox et al. 2016) confirmed that the presence of switchbacks increases dramatically near the Sun (Bale et al. 2019; Kasper et al. 2019) and allowed a thorough study of their characteristics.

Switchbacks have been described as three-dimensional, elongated S-shaped structures with a high aspect ratio in the radial direction (Horbury et al. 2020). The typical deflection angle with respect to the heliospheric magnetic field is broadly distributed (Dudok de Wit et al. 2020), and the duration of the reversals ranges between seconds and hours (Dudok de Wit et al. 2020; Laker et al. 2021). At close distances from the Sun, switchbacks appear in dense, irregular clusters that alternate with quiet periods of stable field polarity and smaller magnetic fluctuations, with a modulation on a timescale of a few hours (Bale et al. 2021). The size and spatial distribution of the switchback patches, as well as the plasma characteristics within them, are compatible with the coronal magnetic structure determined by solar supergranulation (Bale et al. 2021). Switchbacks are associated with enhanced turbulence energy transfer (Bourouaine et al. 2020; Perrone et al. 2020; Hernández et al. 2021; Martinović et al. 2021), and magnetic reconnection was observed at their edges (Froment et al. 2021). On the other hand, because of their limited size, energetic particle propagation along the interplanetary magnetic field does not seem to be affected by their presence (Bandyopadhyay et al. 2021).

It is however expected that switchbacks may play a fundamental role in driving processes that ultimately heat the solar wind. Despite the numerous and thorough experimental studies, the nature of the mechanisms generating the switchbacks is still being debated. For example, it is not clear if they are driven by processes in the lower solar atmosphere (Magyar et al. 2021) or self-consistently generated in the solar wind. While their overall occurrence characteristics observed by PSP so far better support a possible origin in the coronal transition region rather than in situ (Bale et al. 2021; Fargette et al. 2021; Mozer et al. 2021), several competing models have been proposed. For example, switchbacks could be the signature of frequent interchange reconnection events in the solar corona (Veselovsky et al. 1999; Pariat et al. 2009; Fisk & Kasper 2020; Zank et al. 2020; Sterling & Moore 2020; Drake et al. 2021; Liang et al. 2021). According to a different proposed mechanism of coronal generation, they could be associated with the motion of coronal magnetic field footpoints from the slow to the fast wind sectors (Schwadron & McComas 2021). The observed coupling with solar supergranulation (Bale et al. 2021) seems to suggest that switchbacks are nonlinear Alfvénic structures somehow associated with the global circulation of open magnetic flux at the solar surface (Fisk & Kasper 2020; Zank et al. 2021). On the other hand, MHD numerical simulations suggest that switchbacks may be Alfvénic structures originating in the lower corona and propagating out into the heliosphere (Matteini et al. 2015; Tenerani et al. 2020; Jakab & Brandenburg 2021), or may be related to velocity-shear-driven dynamics (Landi et al. 2006; Ruffolo et al. 2020). From the same perspective, switchbacks may be generated self-consistently during the solar wind expansion of turbulent fluctuations (Squire et al. 2020; Shoda et al. 2021).

The variety of proposed models highlights the complex nature of switchbacks, and the limited vantage point provided by single-spacecraft, in situ experimental observations available so far. Remote observation of switchbacks in the corona could provide a more complete description of their spacetime dynamics and help validate the models. However, detecting switchbacks in the extended corona with remote-sensing instruments is challenging and involves high-spatial-resolution coronagraphs. Such an endeavor is further complicated by the absence of coronal magnetic field measurements, so switchbacks can only be revealed by seeking their associated plasma counterparts.

This Letter reports observations from Metis (Antonucci et al. 2020), the coronagraph on board the Solar Orbiter (SO, Müller et al. 2020), showing the first evidence of a magnetic switchback in the solar corona. A thorough data analysis, complemented by a stringent theoretical description and detailed modeling of the event and of the coronal magnetic field, strongly supports the interpretation of the switchback being generated by interchange reconnection between the coronal loops formed above an active region and the nearby open-field regions. This is also particularly relevant to the slow solar wind, whose origin is still widely debated and seems likely to be related to interchange reconnection events continuously occurring at the boundaries between coronal holes and loop systems.

2. Results

2.1. Metis Observations

On 2022 March 25, during SO's first close approach to the Sun at a heliocentric distance of about 0.32 au, the Metis coronagraph observed the solar corona in visible light (580–640 nm), in the annular field of view (FOV) from 1.9 to 3.5

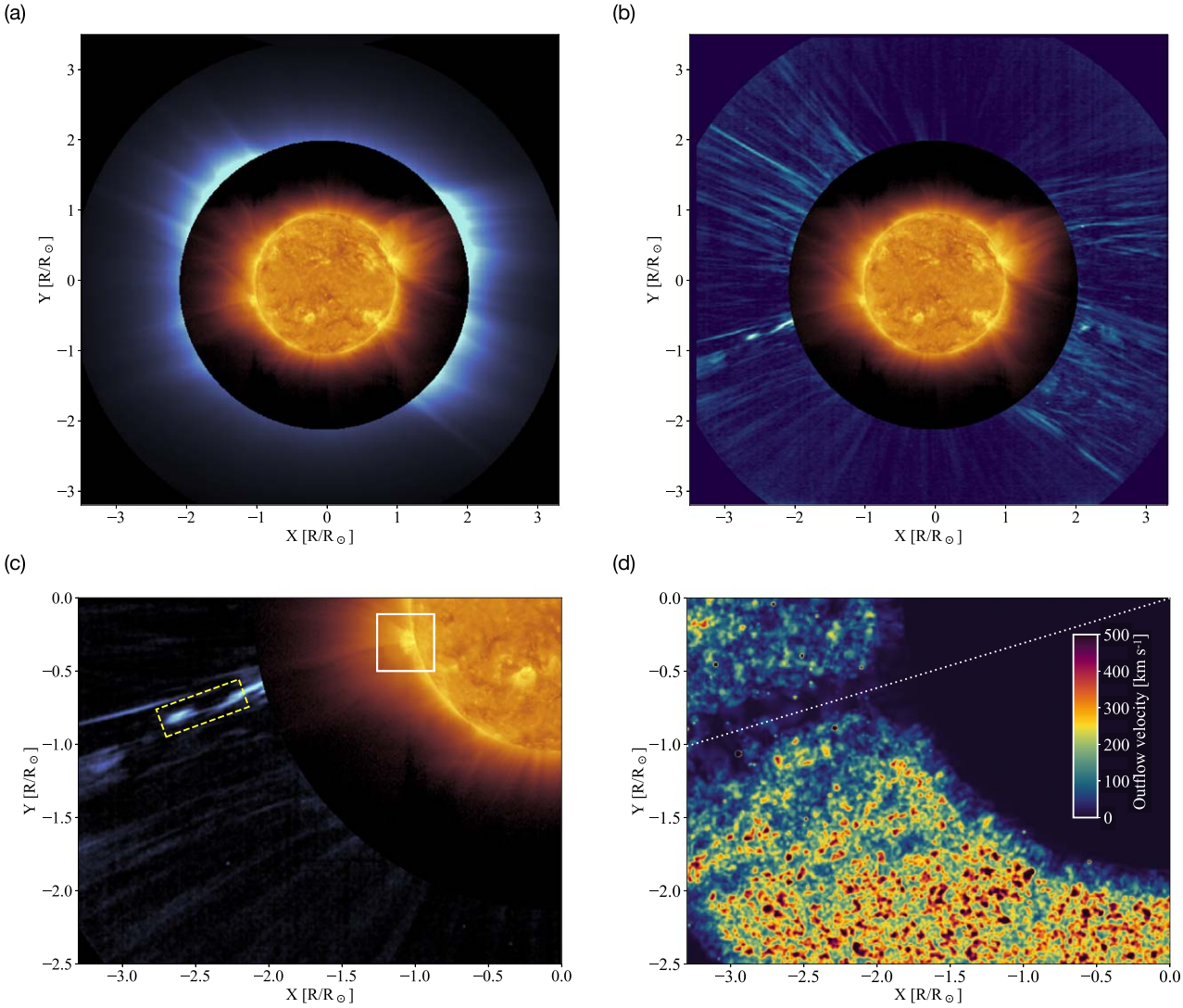

Figure 1. (a) Composite of the Metis-observed tB image of the solar corona within 3.5 $R_\odot$ FOV (blue) and the EUI image of the ultraviolet emission (yellow) as viewed from the SO vantage point on 2022 March 25 at 20:39 UT. (b) Same as in panel (a), but with the Metis observations radially filtered with the SiRGraF algorithm. (c) Zoom-in of panel (b); overlaid is the rectangular ROI where the time–distance analysis on the S-shaped structure was performed, and a white square indicating the loop system associated with AR 12972. (d) Coronal velocity map in the same FOV as in panel (c); the white dotted line marks the latitude relative to the S-shaped feature.

$R_\odot$ ($R_\odot$ = 696 Mm). From 20:11 to 20:52 UT, Metis acquired 120 1024 × 1024 pixel coronal total brightness (tB) images, with a spatial resolution of 4.7 Mm (= 0.0068 $R_\odot$) and time cadence of 20 s. Figure 1(a) displays a composite image of the solar corona on 2022 March 25, at 20:39 UT, obtained by combining the Metis tB image (in blue) with observations from the Extreme Ultraviolet Imager (EUI, Rochus et al. 2020) on SO, taken in ultraviolet light (17.4 nm, in yellow). Figure 1(b) shows the same view of the corona but with the Metis image reprocessed by the Simple Radial Gradient Filter (SiRGraF) algorithm proposed by Patel et al. (2022) to bring out the short-scale dynamic coronal structures. A peculiar S-shaped kink in the stream of plasma flowing off the Sun is clearly visible against the darker coronal background, above the southeastern solar limb. It is worth noting that this coronal feature also emerges by applying independent and different methods, such as a wavelet-based image enhancement algorithm (Telloni et al. 2013) and the Proper Orthogonal Decomposition (POD, Lumley 1981). A zoom of the S-shaped structure is provided in Figure 1(c) and delimited by the rectangular region of interest (ROI). The structure formed above the complex loop system related to the Active Region (AR) 12972 (marked with a white square in the figure). Finally, Figure 1(d) shows the velocity of coronal flows in the same FOV as Figure 1(c). The large-scale coronal flow pattern is derived by tracking outwardly moving density enhancements in the Metis white-light images, via the Fourier Local Correlation Tracking (FLCT; Fisher & Welsch 2008) technique. Noteworthy is the slower plasma stream at latitudes (indicated by a white dotted line) where the S structure occurs.

The sequence of frames in the ROI, displayed in Figure 2 every 400 s from 20:11 UT on 2022 March 25, shows the spatiotemporal evolution of the coronal feature under study. The direction along the structure is oriented horizontally and indicated with altitude above the Sun. The bright structure is observed initially well above the Metis occulted region, forming at a height of about 2.6 $R_\odot$, and then propagates

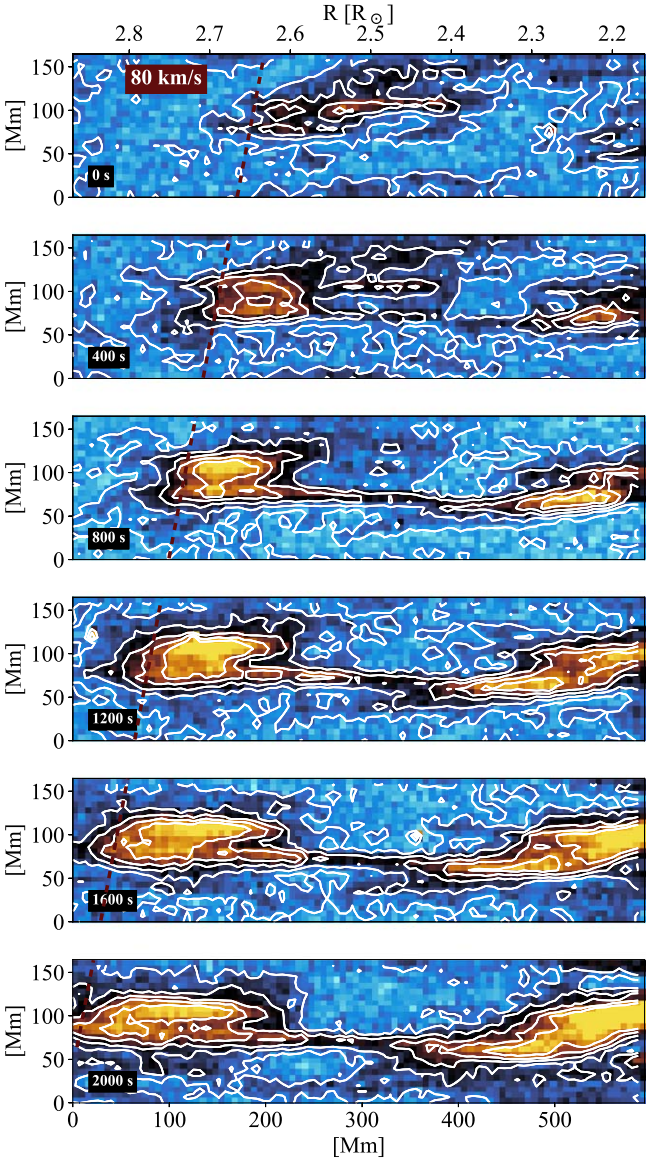

Figure 2. Horizontally-oriented frames of the ROI overlaid in Figure 1(c) every 400 s starting at 20:11 UT on 2022 March 25 (top panel). The upper x-axis indicates the distance from the Sun. The slope of the displayed red dashed line, connecting the radial positions of the main ripple front over time, indicates an almost constant propagation speed of $\sim$80 km s^{-1}.

outward and folds back somewhat. At its full development, the structure acquires the peculiar "S" shape. The time–height plot allows an estimate of the propagation speed of the main ripple, which expands at a constant speed of about 80 km s^{-1} (red dashed line in Figure 2). This is, however, only a lower limit. Indeed, Metis can only estimate the structure's velocity component in the observed plane of the sky (POS), so possible projection effects cannot be ruled out. In addition, the whole structure does not seem to propagate at the same rate, but rather stretches slightly in the radial direction. This could be again due to projection on the POS of a very warped 3D structure or to actual velocity dispersion along the structure. Finally, the Metis images seem to suggest not only an outgoing but also an incoming flow (see, in particular, the frames at 800 and 1200 s after event initiation, where plasma filaments appear to protrude from the main ripple downward), although no firm conclusion can be drawn.

To investigate the vortical properties of the main ripple, which visual inspection seems to suggest, a spectral analysis was performed. Positioning in the rest reference frame of the evolving structure (i.e., at its barycenter) as it propagates outward, its transverse displacements with respect to the radial direction were evaluated. Because it is possible to correlate these transversal displacements with time during the observational period of Metis, a time series of 120 point velocity fluctuations perpendicular to the structure can thus be obtained. The corresponding Fourier power spectral density (Figure 3) shows clearly that there is a single dominant frequency (at 12 mHz) with some sideband noise or less important fluctuations. Because 12 mHz is not a common frequency, it is likely to be an intrinsic kink mode of the structure. It follows that the characteristic timescale of the vortex roll is about 80 seconds. Hence, the ripple is essentially nonturbulent in nature, because otherwise a broadband spectrum should have been found.

2.2. Coronal Magnetic Field Modeling

The large-scale configuration of the coronal magnetic field during the observation period and, most importantly, the local magnetic topology around the active region above which the S-shaped structure appears to emerge are of crucial importance for context and for proper interpretation of the results obtained from the Metis data. A magnetic field reconstruction is accomplished by applying the 3D MHD model developed by Predictive Science Incorporated (PSI) and based on the wave-turbulence-driven (WTD) heating approach (Mikić et al. 2018).

The photospheric boundary conditions used for the extrapolation rely on Carrington maps of the measurements from the Helioseismic and Magnetic Imager (HMI, Scherrer et al. 2012) on board the Solar Dynamics Observatory (SDO, Pesnell et al. 2012). In the region of interest, observed at the east limb on 2022 March 25, the magnetic field map resolution is improved by including data segments of high-resolution HMI vector data. The modeled magnetic field lines traced on the Metis POS are displayed (along with the open flux regions on the solar surface) in Figure 4(a). The squashing factor Q (Titov et al. 2011), which highlights the separatrix arcs of the 3D coronal magnetic field, is imaged in Figure 4(b). The separatrix web, made up of the separatrix and quasi-separatrix layers surrounding the heliospheric current sheet (HCS), can be better visualized by building maps of log Q at 3 $R_\odot$ (Figure 4(c)). In these layers, the photospheric dynamics stresses the separatrices, inducing current sheets and reconnection processes with the subsequent release of coronal plasma. The released plasma is proposed to contribute to the slow wind observed in the heliosphere in the zones around the current sheet (Antiochos et al. 2012). West of AR 12972 (located exactly at the heliographic coordinates of the Metis-observed S-shaped feature), the separatrix between a tiny positive coronal hole, which is connected to the active region and touches the HCS, and a larger positive coronal hole has the signature of a null where they collide with the HCS. A pseudostreamer (PS) separatrix curtain lies east of the active region. Figures 4(d) and (e) finally show the synoptic maps of the photospheric radial magnetic field and of the footprints of the field lines associated with outward (red) and inward (blue) open flux at 3 $R_\odot$. A small patch of open-field lines can be identified at the active region location.

What clearly emerges from the MHD extrapolation of the global and local magnetic field is the complex loop system

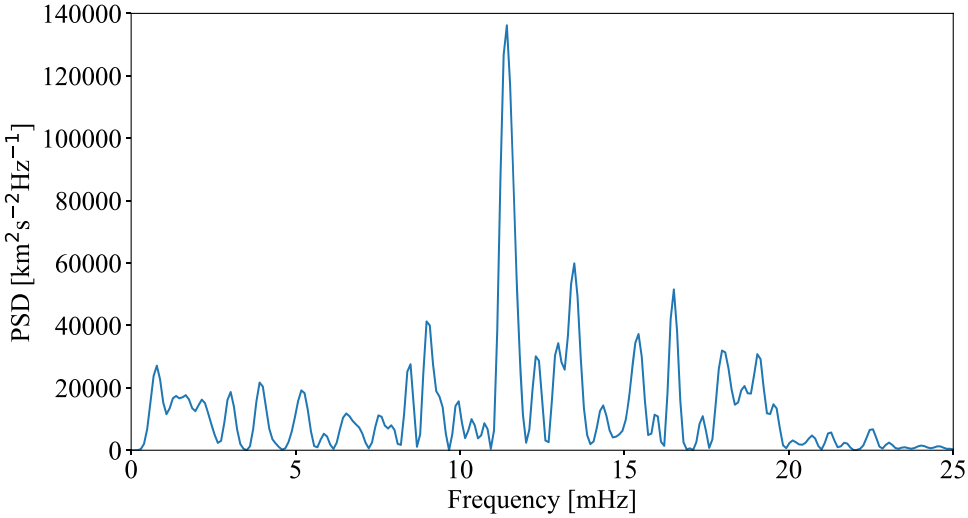

Figure 3. Power spectral density of velocity fluctuations transverse to the main ripple propagation direction. A characteristic 12 mHz frequency emerges clearly.

above the active region and the large magnetic arcs extending up to 2–3 $R_\odot$ in the FOV of Metis, just where the S-shaped vortical structure forms. More interestingly, the active region appears to be surrounded, both east and west, by open-field regions injecting plasma along the coronal plasma sheet. Essentially, the large helmet streamer formed above AR 12972 is broken up slightly by the fluxes/thermodynamics of the strong ARs. This is vital to the interpretation of the nature and source mechanism of the kink-like structure observed with Metis, as discussed below.

3. Discussion

3.1. Switchback Driven by Interchange Reconnection

Based on Metis measurements, the previous section has provided observational evidence of the shape of a plasma structure in the solar corona, the height at which it was formed, the way it was generated, its spatiotemporal evolution, its vortical properties, the local magnetic field topology associated with an underlying active region, and the coupling of the structure with a slow coronal plasma flow. As will be argued in the following, all this evidence concurs in supporting the interpretation of the observed structure as a magnetic switchback generated in the solar corona through interchange reconnection.

The process of magnetic reconnection of a loop and an open-field line, known as interchange reconnection, may occur at the boundaries between closed- and open-field regions at the streamer–coronal hole interface, and at the edges of active regions surrounded by unipolar regions or small coronal holes. The mechanism is depicted in the cartoon in Figure 3 of Zank et al. (2020). Interchange reconnection events can trigger the formation of magnetic field deflections, which propagate both outward and inward, whenever they are launched in the sub-Alfvénic flow (Zank et al. 2020). The most extreme switchbacks take the characteristic S shape and are detected in situ as magnetic field reversals. The launch of switchbacks could also be accompanied by coronal jets (Sterling & Moore 2020). As a result of interchange reconnection, coronal plasma can be additionally released as blobs or plasmoids in the solar wind (Sheeley et al. 1997; Wang et al. 1998). The switchback generated by such a mechanism (likely higher up in the corona, between large-scale loops and the adjacent open-field lines surrounding an active region) will hence be a single structure characterized by a perturbed magnetic field having a wavy shape. It will be associated with upward and potentially also downward flow of plasma that is different from the coronal background. In addition, such a switchback will consist of a single characteristic mode.

All of these expected characteristics are actually depicted in the Metis images investigated here. First, the observed structure is S shaped (Figure 1(c)). If the direction of the flow is thought to be controlled by the strong coronal magnetic field, the white-light enhancement can be used as a way to infer the magnetic field direction. Thus, an S-shaped enhancement can be associated with an S-shaped magnetic field region. Second, the time–distance maps in Figure 2 indicate the observation of both switchback-related forward and inward flows, as predicted by Zank et al. (2020). Third, the observed coronal feature originates exactly above AR 12972 (Figure 4(d)), whose loop system, extending well above the Metis occulter, is surrounded by open-field regions, as shown by magnetic field extrapolations (Figure 4(e)). Thus, it appears to be the ideal site for an interchange reconnection event to launch a switchback. Furthermore, the switchback-associated plasma is denser than the surrounding ambient corona (Figure 1(c)), probably due to the compressions associated with the magnetic reconnection process and/or the entrapment of denser loop material. And, finally, the observation that the presumed switchback forms at a high altitude in the solar corona[35] is suggested by the possible location of the separatrix field lines at the null point (as well as by the squashing factor synoptic map displayed in Figure 4(c)). Fourth, observation of the single well-defined structure in Metis images rules out a shear-related Kelvin–Helmholtz (KH) type of driving (as proposed by Ruffolo et al. 2020) and favors the interchange reconnection scenario. Indeed, a KH instability would not generate one large single propagating vortex, but rather multiple spatially distributed structures along the shear flow, many of which could be expected to be closely spaced or even interacting (as at the CME flank observed by Foullon et al. 2011, and in striking contrast to Metis observations). Fifth, the presence of a single dominant timescale (Figure 3)

[35] No propagating intensity disturbances in the inner corona were observed by EUI at that time.

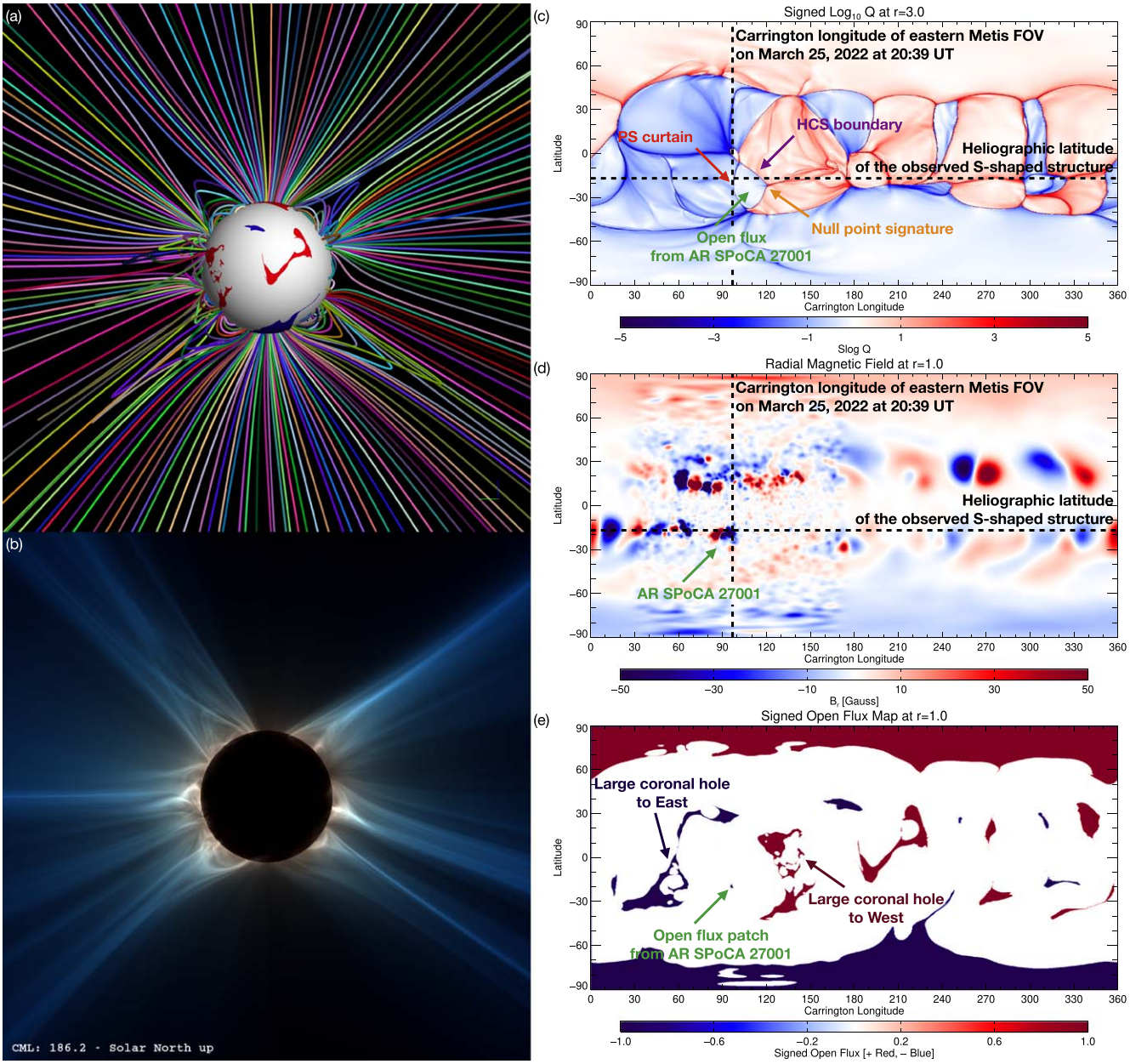

Figure 4. Modeled magnetic field lines (a) and rendered squashing factor Q (b) from the SO point of view on 2022 March 25. Carrington maps of $\log Q$ at 3 $R_\odot$ (c), photospheric radial magnetic field (d), and open-field regions on the Sun's surface (e). The Carrington longitude of the eastern Metis FOV on 2022 March 25 at 20:39 UT and the heliographic latitude of the observed S-shaped structure are marked by the black vertical and horizontal dashed lines, respectively. AR 12972 and the associated open flux are indicated by a green arrow. The latter maps to the PS curtain and the HCS (as indicated by color-coded arrows) in several places in latitude and longitude, forming a null-point signature (denoted by the orange arrow).

characterizing the observed ripple is consistent with a nonturbulent description of the switchback (as in the model by Zank et al. 2020 and Liang et al. 2021). This is not compatible with the KH origin of switchbacks, or with the idea that switchbacks are a natural outcome of evolving turbulence in an expanding flow (as advanced by Squire et al. 2020). Indeed, in both cases, switchbacks would include a superposition of modes mutually interacting nonlinearly, thus generating a turbulent flow, without a characteristic dominant frequency. According to this analysis, the structure observed by Metis looks like a very clear switchback initiated by an interchange reconnection event occurring above an active region higher up in corona.

To conclude, adopting the perspective that interchange reconnection generates a switchback and then asking what the observational and theoretical support might be once that hypothesis is adopted, support for the existence of switchbacks in the solar corona generated by interchange reconnection can be argued from both observational and theoretical perspectives.

3.2. Switchback Modeling

To provide further clues to support the proposed interpretation and possibly to empirically validate the theoretical predictions by Zank et al. (2020) against the Metis observations, the spatio-temporal evolution of the observed switchback structure was

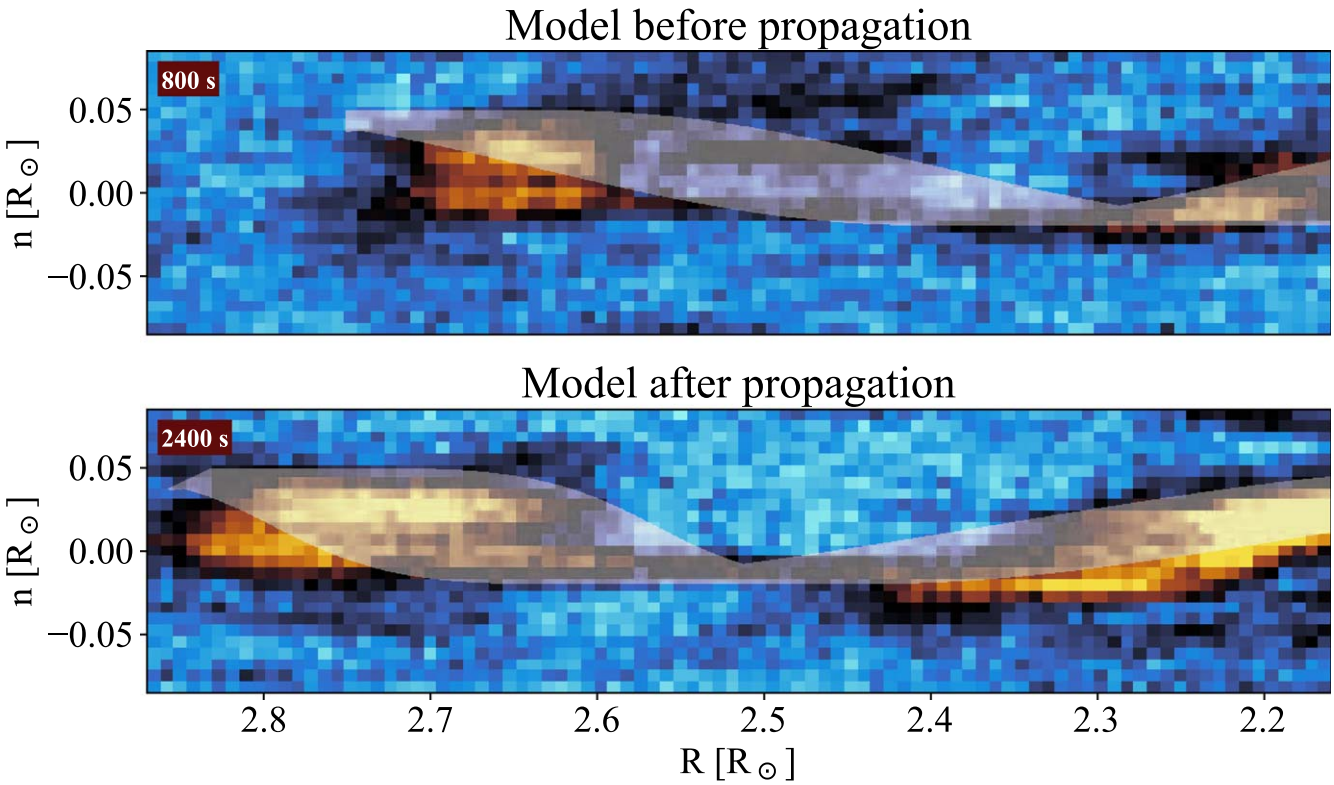

Figure 5. MCMC-modeled switchback (white shape) before and after linear-theory-based propagation, compared with Metis observations at 800 and 2400 s after initiation.

modeled using the Markov Chain Monte Carlo (MCMC) method. The shape of the structure was initially modeled with a sinusoidal function $n - n_0 = A \sin[b(r - r_0)]$, where n and r are the positions in heliographic coordinates, n_0 and r_0 are the shifts in the n and r directions, respectively, A is the amplitude of the perturbation in n, b is the wavenumber of the sinusoidal function, and d is a factor adjusting the width of the structure along the r direction, i.e., $\left| r - r_0 - \frac{1}{b}\arcsin\left(\frac{n - n_0}{A}\right) \right| < \frac{d}{2}$. In addition, to simulate the flow shear in the surrounding solar wind, a velocity gradient varying as $n(U_r(n) = kn + U_0$, where $U_r(n)$ is the background solar wind speed, U_0 is a reference speed, and k denotes the slope of the flow velocity), was also included. For simplicity, only the propagation in r was considered. The initial structure was then allowed to evolve, based on the linear-theory propagation function by Zank et al. (2020). The shape of the propagated structure was finally compared with Metis observations at 2400 s after the switchback initiation, using the MCMC technique. The MCMC method is based on Bayesian inference (e.g., Bonamente 2013) and was used to provide the most probable values of the free parameters n_0, r_0, A, b, d, and k that lead to the optimal fit of the model to the observations (this approach has been successfully applied in heliospheric studies by Zhao et al. 2019 and Liang et al. 2021, where the interested reader can find more details on the application of the MCMC technique). The results are displayed in Figure 5, where the modeled switchback shape before and after propagation (white shape) is overlaid on the Metis image 800 and 2400 s after the switchback formation.

Although the model obviously cannot capture all features of the imaged switchback, the agreement with observations is striking. In particular, the modeled switchback elongates during propagation, which is consistent with the observations. Even more remarkable is that although the free parameters were set to best reproduce the shape of the 2400 s switchback, the 800 s structure so modeled also fits satisfactorily the observations. This is a strong indication of the validity of the linear theory proposed by Zank et al. (2020) to describe the propagation of switchbacks in the corona and greatly supports the scenario of having identified a magnetic switchback low in the solar corona for the first time.

3.3. Switchbacks and the Slow Solar Wind

The observation of switchbacks in the solar corona is closely related to the still-unsolved problem of the origin of the slow solar wind. Indeed, one of the possible mechanisms for the origin of the slow coronal flows is that initially proposed by Fisk et al. (1999) and Fisk (2003) and later extended by Zank et al. (2021) by incorporating a mechanism for plasma heating. In this model (well illustrated in Figure 1 of Zank et al. 2021), the large-scale loop plasma is heated to high temperatures via the dissipation of quasi 2D turbulence generated by the magnetic carpet. An interchange reconnection event with an open-field line at altitudes of 2–4 $R_\odot$ liberates the already hot loop plasma onto an open-field coronal region, which then expands to reach supersonic and super-Alfvénic speeds. It appears thus evident that switchbacks and slow solar wind streams can be viewed as two manifestations of the same physical process, i.e., interchange reconnection. A number of clues supporting this possible scenario are present in the literature. For instance, the speed of the coronal blobs released by reconnection events (Sheeley et al. 1997; Wang et al. 1998) was found to be consistent with that of the slow wind (Antonucci et al. 2005). Actually, quantifying the contribution of reconnection-related coronal blobs to the slow wind plasma

has been the subject of several studies over the past decade (e.g., Antiochos et al. 2012; Wang 2012, 2020). Furthermore, Harra et al. (2008), Brooks & Warren (2011), Del Zanna et al. (2011), Fazakerley et al. (2016), and Harra et al. (2017) observed persistent coronal plasma upflows in association with quiescent active regions (first identified by Uchida et al. 1992) and interpreted this evidence as an indication of magnetic reconnection being the main driver of the slow wind. Furthermore, slow coronal flows have been observed to originate at the edges of coronal holes adjacent to closed-configuration equatorial streamers, and then stream along their flanks (Antonucci et al. 2005). Finally, switchbacks are not observed in the middle of low-speed streams because, again in the interchange reconnection picture, these can only occur at the boundaries of slow and fast wind. Because both the loop system and the open-field region consist of multiple magnetic field lines, interchange reconnection can occur in rapid succession, resulting in clustering of switchbacks (consistent with PSP measurements; e.g., Dudok de Wit et al. 2020) and in steady slow coronal flows. This process will continue while the loop system keeps emerging from the active region and until the magnetic footpoint motions ensure that the closed- and open-field regions are close enough to magnetically reconnect. Hence, the timing of the coronal switchback observed with Metis, as well as the height of its initiation, may be indicators of the origin of slow solar wind. As discussed in the previous section (Figures 1(d) and 2), the switchback is observed to form at about 2.6 $R_{\odot}$ and then expand at the low speed of $\sim$80 km s^{-1} in a plasma stream slower than the adjacent ones. A remarkable relation of the switchback formation with the coronal region of slow plasma outflows has therefore been found, interestingly converging toward the interchange reconnection interpretation. Therefore, the study of switchbacks in the corona, especially where, how, and how often they are formed, seems to be very promising in disclosing the origin of the slow solar wind.

Solar Orbiter is a space mission of international collaboration between ESA and NASA, operated by ESA. D.T. was partially supported by the Italian Space Agency (ASI) under contract 2018-30-HH.0. G.P.Z., H.L., M.N., L.A., and L.-L.Z. acknowledge the partial support of NASA Parker Solar Probe contract SV4-84017, an NSF EPSCoR RII-Track-1 Cooperative Agreement OIA-1655280, and a NASA IMAP grant through SUB000313/80GSFC19C0027. L.S.-V. was funded by the SNSA grants 86/20 and 145/18. L.P.C. gratefully acknowledges funding by the European Union. Views and opinions expressed are however those of the author(s) only and do not necessarily reflect those of the European Union or the European Research Council (grant agreement 101039844). Neither the European Union nor the granting authority can be held responsible for them. D.M.L. is supported by STFC Ernest Rutherford fellowship ST/R003246/1. S.P. acknowledges the funding by CNES through the MEDOC data and operations center. The Royal Observatory of Belgium team thanks the Belgian Federal Science Policy Office (BELSPO) for the provision of financial support in the framework of the PRODEX program of ESA under contract numbers 4000134474 and 4000136424. The Metis program is supported by ASI under contracts to the National Institute for Astrophysics and industrial partners. Metis was built with hardware contributions from Germany (Bundesministerium für Wirtschaft und Energie through the Deutsches Zentrum für Luft- und Raumfahrt e.V.), the Czech Republic (PRODEX) and ESA. The EUI instrument was built by CSL, IAS, MPS, MSSL/UCL, PMOD/WRC, ROB, LCF/IO with funding from the Belgian Federal Science Policy Office (BELSPO/PRODEX PEA 4000134088, 4000112292, 4000117262, and 4000134474); the Centre National dÉtudes Spatiales (CNES); the UK Space Agency (UKSA); the Bundesministerium für Wirtschaft und Energie (BMWi) through Deutsches Zentrum für Luft- und Raumfahrt (DLR); and the Swiss Space Office (SSO). The Metis data analyzed in this paper are available from the PI on request. "EUI Data Release 5.0 2022-04" is public and can be freely downloaded from the EUI website (https://www.sidc.be/EUI/data/) and from the Solar Orbiter Archive (http://soar.esac.esa.int/soar/). Inquiries regarding the coronal magnetic field extrapolation and the switchback modeling shown in the present study can be addressed to Cooper Downs (e-mail: cdowns@predsci.com) and Haoming Liang/Masaru Nakanotani (e-mails: hl0045@uah.edu; mn0052@uah.edu), respectively.

ORCID iDs

Daniele Telloni https://orcid.org/0000-0002-6710-8142
Gary P. Zank https://orcid.org/0000-0002-4642-6192
Marco Stangalini https://orcid.org/0000-0002-5365-7546
Cooper Downs https://orcid.org/0000-0003-1759-4354
Haoming Liang https://orcid.org/0000-0001-9581-4821
Masaru Nakanotani https://orcid.org/0000-0002-7203-0730
Vincenzo Andretta https://orcid.org/0000-0003-1962-9741
Ester Antonucci https://orcid.org/0000-0003-4155-6542
Luca Sorriso-Valvo https://orcid.org/0000-0002-5981-7758
Laxman Adhikari https://orcid.org/0000-0003-1549-5256
Lingling Zhao https://orcid.org/0000-0002-4299-0490
Raffaele Marino https://orcid.org/0000-0002-6433-7767
Roberto Susino https://orcid.org/0000-0002-1017-7163
Catia Grimani https://orcid.org/0000-0002-5467-6386
Michele Fabi https://orcid.org/0000-0002-2464-1369
Raffaella D'Amicis https://orcid.org/0000-0003-2647-117X
Denise Perrone https://orcid.org/0000-0003-1059-4853
Roberto Bruno https://orcid.org/0000-0002-2152-0115
Francesco Carbone https://orcid.org/0000-0002-3559-5273
Salvatore Mancuso https://orcid.org/0000-0002-9874-2234
Marco Romoli https://orcid.org/0000-0001-9921-1198
Vania Da Deppo https://orcid.org/0000-0001-6273-8738
Silvano Fineschi https://orcid.org/0000-0002-2789-816X
Petr Heinzel https://orcid.org/0000-0002-5778-2600
John D. Moses https://orcid.org/0000-0001-9670-2063
Giampiero Naletto https://orcid.org/0000-0003-2007-3138
Gianalfredo Nicolini https://orcid.org/0000-0002-9459-3841
Daniele Spadaro https://orcid.org/0000-0003-3517-8688
Luca Teriaca https://orcid.org/0000-0001-7298-2320
Federica Frassati https://orcid.org/0000-0001-9014-614X
Giovanna Jerse https://orcid.org/0000-0002-0764-7929
Federico Landini https://orcid.org/0000-0001-8244-9749
Maurizio Pancrazzi https://orcid.org/0000-0002-3789-2482
Giuliana Russano https://orcid.org/0000-0002-2433-8706
Clementina Sasso https://orcid.org/0000-0002-5163-5837
Ruggero Biondo https://orcid.org/0000-0002-3929-016X
Aleksandr Burtovoi https://orcid.org/0000-0002-8734-808X
Giuseppe E. Capuano https://orcid.org/0000-0002-8430-8218
Chiara Casini https://orcid.org/0000-0001-8783-0047
Marta Casti https://orcid.org/0000-0002-9716-3820
Paolo Chioetto https://orcid.org/0000-0002-3379-2142

Yara De Leo https://orcid.org/0000-0003-2426-2112
Marina Giarrusso https://orcid.org/0000-0002-4453-1597
Alessandro Liberatore https://orcid.org/0000-0002-0016-7594
David Berghmans https://orcid.org/0000-0003-4052-9462
Frédéric Auchère https://orcid.org/0000-0003-0972-7022
Regina Aznar Cuadrado https://orcid.org/0000-0003-1294-1257
Lakshmi P. Chitta https://orcid.org/0000-0002-9270-6785
Louise Harra https://orcid.org/0000-0001-9457-6200
Emil Kraaikamp https://orcid.org/0000-0002-2265-1803
David M. Long https://orcid.org/0000-0003-3137-0277
Sudip Mandal https://orcid.org/0000-0002-7762-5629
Susanna Parenti https://orcid.org/0000-0003-1438-1310
Gabriel Pelouze https://orcid.org/0000-0002-0397-2214
Hardi Peter https://orcid.org/0000-0001-9921-0937
Luciano Rodriguez https://orcid.org/0000-0002-6097-374X
Udo Schühle https://orcid.org/0000-0001-6060-9078
Conrad Schwanitz https://orcid.org/0000-0002-7669-5078
Phil J. Smith https://orcid.org/0000-0002-3281-4223
Cis Verbeeck https://orcid.org/0000-0002-5022-4534
Andrei N. Zhukov https://orcid.org/0000-0002-2542-9810

References

Antiochos, S. K., Linker, J. A., Lionello, R., et al. 2012, SSRv, 172, 169
Antonucci, E., Abbo, L., & Dodero, M. A. 2005, A&A, 435, 699
Antonucci, E., Romoli, M., Andretta, V., et al. 2020, A&A, 642, A10
Bale, S. D., Badman, S. T., Bonnell, J. W., et al. 2019, Natur, 576, 237
Bale, S. D., Horbury, T. S., Velli, M., et al. 2021, ApJ, 923, 174
Balogh, A., Forsyth, R. J., Lucek, E. A., Horbury, T. S., & Smith, E. J. 1999, GeoRL, 26, 631
Bandyopadhyay, R., Matthaeus, W. H., McComas, D. J., et al. 2021, A&A, 650, L4
Bonamente, M. 2013, Statistics and Analysis of Scientific Data (New York: Springer)
Bourouaine, S., Perez, J. C., Klein, K. G., et al. 2020, ApJL, 904, L30
Brooks, D. H., & Warren, H. P. 2011, ApJL, 727, L13
Bruno, R., & Carbone, V. 2013, LRSP, 10, 2
Del Zanna, G., Aulanier, G., Klein, K. L., & Török, T. 2011, A&A, 526, A137
Drake, J. F., Agapitov, O., Swisdak, M., et al. 2021, A&A, 650, A2
Dudok de Wit, T., Krasnoselskikh, V. V., Bale, S. D., et al. 2020, ApJS, 246, 39
Fargette, N., Lavraud, B., Rouillard, A. P., et al. 2021, ApJ, 919, 96
Fazakerley, A. N., Harra, L. K., & van Driel-Gesztelyi, L. 2016, ApJ, 823, 145
Fisher, G. H., & Welsch, B. T. 2008, in ASP Conf. Ser. 383, Subsurface and Atmospheric Influences on Solar Activity, ed. R. Howe, R. W. Komm, K. S. Balasubramaniam, & G. J. D. Petrie (San Franciso,CA: ASP), 373
Fisk, L. A. 2003, JGRA, 108, 1157
Fisk, L. A., & Kasper, J. C. 2020, ApJL, 894, L4
Fisk, L. A., Schwadron, N. A., & Zurbuchen, T. H. 1999, JGRA, 104, 19765
Foullon, C., Verwichte, E., Nakariakov, V. M., Nykyri, K., & Farrugia, C. J. 2011, ApJL, 729, L8
Fox, N. J., Velli, M. C., Bale, S. D., et al. 2016, SSRv, 204, 7
Froment, C., Krasnoselskikh, V., Dudok de Wit, T., et al. 2021, A&A, 650, A5
Harra, L. K., Sakao, T., Mandrini, C. H., et al. 2008, ApJL, 676, L147
Harra, L. K., Ugarte-Urra, I., De Rosa, M., et al. 2017, PASJ, 69, 47
Hernández, C. S., Sorriso-Valvo, L., Bandyopadhyay, R., et al. 2021, ApJL, 922, L11
Horbury, T. S., Matteini, L., & Stansby, D. 2018, MNRAS, 478, 1980
Horbury, T. S., Woolley, T., Laker, R., et al. 2020, ApJS, 246, 45
Hundhausen, A. J. 1972, Coronal Expansion and Solar Wind (Berlin: Springer)
Jakab, P., & Brandenburg, A. 2021, A&A, 647, A18
Kasper, J. C., Bale, S. D., Belcher, J. W., et al. 2019, Natur, 576, 228
Laker, R., Horbury, T. S., Bale, S. D., et al. 2021, A&A, 650, A1
Landi, S., Hellinger, P., & Velli, M. 2006, GeoRL, 33, L14101
Liang, H., Zank, G. P., Nakanotani, M., & Zhao, L. L. 2021, ApJ, 917, 110
Lumley, J. L. 1981, in Transition and Turbulence (New York: Academic Press), 215
Magyar, N., Utz, D., Erdélyi, R., & Nakariakov, V. M. 2021, ApJ, 911, 75
Martinović, M. M., Klein, K. G., Huang, J., et al. 2021, ApJ, 912, 28
Matteini, L., Horbury, T. S., Pantellini, F., Velli, M., & Schwartz, S. J. 2015, ApJ, 802, 11
Mikić, Z., Downs, C., Linker, J. A., et al. 2018, NatAs, 2, 913
Mozer, F. S., Bale, S. D., Bonnell, J. W., et al. 2021, ApJ, 919, 60
Müller, D., St., Cyr, O. C., Zouganelis, I., et al. 2020, A&A, 642, A1
Pariat, E., Antiochos, S. K., & DeVore, C. R. 2009, ApJ, 691, 61
Patel, R., Majumdar, S., Pant, V., & Banerjee, D. 2022, SoPh, 297, 27
Perrone, D., Bruno, R., D'Amicis, R., et al. 2020, ApJ, 905, 142
Pesnell, W. D., Thompson, B. J., & Chamberlin, P. C. 2012, SoPh, 275, 3
Rochus, P., Auchère, F., Berghmans, D., et al. 2020, A&A, 642, A8
Ruffolo, D., Matthaeus, W. H., Chhiber, R., et al. 2020, ApJ, 902, 94
Scherrer, P. H., Schou, J., Bush, R. I., et al. 2012, SoPh, 275, 207
Schwadron, N. A., & McComas, D. J. 2021, ApJ, 909, 95
Sheeley, N. R., Wang, Y. M., Hawley, S. H., et al. 1997, ApJ, 484, 472
Shoda, M., Chandran, B. D. G., & Cranmer, S. R. 2021, ApJ, 915, 52
Squire, J., Chandran, B. D. G., & Meyrand, R. 2020, ApJL, 891, L2
Sterling, A. C., & Moore, R. L. 2020, ApJL, 896, L18
Telloni, D., Ventura, R., Romano, P., Spadaro, D., & Antonucci, E. 2013, ApJ, 767, 138
Tenerani, A., Velli, M., Matteini, L., et al. 2020, ApJS, 246, 32
Titov, V. S., Mikić, Z., Linker, J. A., Lionello, R., & Antiochos, S. K. 2011, ApJ, 731, 111
Uchida, Y., McAllister, A., Strong, K. T., et al. 1992, PASJ, 44, L155
Veselovsky, I. S., Zhukov, A. N., Koutchmy, S., Delannée, C., & Delaboudinière, J. P. 1999, in ESA Special Publication, VIII SOHO Workshop: Plasma Dynamics and Diagnostics in the Solar Transition Region and Corona 446, ed. J. C. Vial & B. Kaldeich-Schümann (Paris: ESA Special Publications), 675
Wang, Y. M. 2012, SSRv, 172, 123
Wang, Y. M. 2020, ApJ, 904, 199
Wang, Y. M., Sheeley, N. R. J., Walters, J. H., et al. 1998, ApJL, 498, L165
Yamauchi, Y., Suess, S. T., Steinberg, J. T., & Sakurai, T. 2004, JGRA, 109, A03104
Zank, G. P., Nakanotani, M., Zhao, L. L., Adhikari, L., & Kasper, J. 2020, ApJ, 903, 1
Zank, G. P., Zhao, L. L., Adhikari, L., et al. 2021, PhPl, 28, 080501
Zhao, L. L., Zank, G. P., Hu, Q., et al. 2019, ApJ, 886, 144